OPTIMAL ORIENTATION DETECTION OF LINEAR SYMMETRY*

Josef Bigün, Gösta H. Granlund
Linköping University
Department of Electrical Engineering
Computer Vision Laboratory
S-581 83 Linköping Sweden

Abstract

The problem of optimal detection of orientation in arbitrary neighbourhoods is solved in the least squares sense. It is shown that this corresponds to fitting an axis in the Fourier domain of the n–dimensional neighbourhood, the solution of which is a well known solution of a matrix eigenvalue problem. The eigenvalues are the variance or inertia with respect to the axes given by their respective eigenvectors. The orientation is taken as the axis given by the least eigenvalue. Moreover it is shown that the necessary computations can be performed in the spatial domain without doing a Fourier transformation. An implementation for 2–D is presented. Two certainty measures are given, corresponding to the orientation estimate. These are the relative or the absolute distances between the two eigenvalues, stating whether the fitted axis is much better than an axis orthogonal to it. The result of the implementation is verified by experiments which confirm an accurate orientation estimation and reliable certainty measure in the presence of additive noise at high as well as low level.

1 Introduction

The problem of orientation detection of lines and edges arises in many applications in image processing. One of the earliest approaches was to model the direction of a neighbourhood in terms of the direction of the gradient of the image. A drawback of this method is its noise amplification since the gradient operation enhances high frequencies of the image. Another approach is to combine linearly the magnitudes of a number, 3 or 4, of quadrature, directional filters, [1]. The coefficients in this linear functional are complex valued as well as those of the filters. This results in a complex valued variable, the argument of which

*©PROCEEDINGS OF THE IEEE FIRST INTERNATIONAL CONFERENCE ON COMPUTER VISION, London, June 8-11, IEEE Computer Society Press, pp. 433-438, 1987.

is an estimate of the orientation of the local neighbourhood and the magnitude is an estimate of the certainty of this orientation estimation. There have also been solutions to the problem of finding the local orientation by projecting the neighbourhood to a number of fixed orthogonal functions. The projection coefficients are then used to evaluate the orientation parameter of the model [2,3].
We will propose a new approach for local orientation detection which is based on the well-known solution of the principal axis problem of rigid bodies in mechanics, but applied in the Fourier domain [5, 6,10]. In Section 1, we will define linear symmetry and describe the method for an n–dimensional Euclidean space. In Section 2 we will apply the results for 2–dimensional images and in Section 3 the experiments and results for the 2–D case will be presented. We predict that the experimental results of this approach for the 3–D case should be similar to those for 2–D. Since lines and edges are linear symmetric structures, this method can be used for detection of these structures by means of the certainty parameters introduced in Section 2, as well as orientation estimation in applications.

2 Orientation detection in n-dimensional Euclidean space.

Let E_n be the Euclidean space with dimension n.

Definition 1 *We will call a non–negative and bounded function f with real or complex values defined on E_n an image, and the values of f the gray values of the image. Further we will call an image linearly symmetric if the isogray values constitute parallel hyperplanes of dimension $n-1$. That is if the image f can be expressed by a function g defined on E_1 for some vector $\bar{k} \in E_n$ as $f(\bar{r}) = g(\bar{k} \cdot \bar{r})$ for all $\bar{r} \in E_n$.*

Theorem 1 *A linear symmetric image has a Fourier transform concentrated to a line through the origin:*

$$\mathcal{F}_n(f(\bar{k}_0^t \bar{r}))(\bar{s}) = \mathcal{F}_1(f)(\bar{s}^t \bar{k}_0)\delta(\bar{s}^t \bar{u}_1)\delta(\bar{s}^t \bar{u}_2)\cdots\delta(\bar{s}^t \bar{u}_{n-1})$$

$\bar{k}_0, \bar{u}_1 ... \bar{u}_{n-1}$ are orthonormal, and δ is the dirac distribution.

Proof: Decompose E_n in E_1 and E_{n-1}

$$\bar{r} = t\bar{k}_o + u_2\bar{u}_1 + u_2\bar{u}_2 .... u_{n-1}\bar{u}_{n-1}$$

for all $\bar{r} \in E_n$, so that $\bar{k}_0$, $\bar{u}_1$, $\bar{u}_2$ ... $\bar{u}_{n-1}$ are orthonormal.

$$\mathcal{F}_n(f(\bar{k}^t \bar{r})) = \int_{-\infty}^{\infty} \cdots \int_{-\infty}^{\infty} f(t) \exp(-\jmath 2\pi t \bar{s}^t \bar{k}_0) \times$$
$$\exp\left(-\jmath 2\pi (\bar{s}^t \bar{u}_1, u_1 + \bar{s}^t \bar{u}_2 u_2 ... \bar{s}^t \bar{u}_{n-1} u_{n-1})\right) dt du_1 \cdots du_{n-1}$$

then the desired result follows immediately.

To detect linearly symmetric objects is consequently the same as to check the existence of energy concentration to a line in the Fourier domain. This theorem further states that the function $f(\bar{k}_0^t \bar{r})$, which is in general a "spread" function, is compressed to a line. This is a property which supports the idea of checking the linear symmetry in the Fourier domain rather than in the spatial domain. But the Fourier transformation of every local neighbourhood is very cumbersome. We will show that the fitting of a straight line through the origin in the Fourier domain of an image with the least square error is possible to accomplish in the spatial domain. If we define the infinitesimal energy of the Fourier transform, $|\hat{f}(\bar{r})|^2 dE_n$, as the mass distribution, then we have the variance (or the inertia) with respect to the axis $t\bar{k}_0$

$$V_f^2 = \int_{\bar{r} \in E_n} d^2(\bar{r}, \bar{k}_0) dm(\bar{r}) \tag{1}$$

for the Fourier transform of the image, f. Here $d(\bar{r}, \bar{k}_0)$ is a real valued function which gives the Euclidean distance between the point $\bar{r}$ and a candidate axis, defined by the axis $t\bar{k}_0$, where $\|\bar{k}_0\| = 1$. The problem is to find such an axis minimizing V_f^2:

$$\min V_f^2 = \min \int_{E_n} d^2(\bar{r}, \bar{k}_0) |\hat{f}(\bar{r})|^2 dE_n \tag{2}$$

where dE_n is $dx_1 dx_1 \cdots dx_n$ when $\bar{r} = x_1.\hat{x}_1 + \hat{x}_2 ... x_n \hat{x}_n$ for all $\bar{r} \in E_n$. The distance function is given by the usual Euclidean distance:

$$\begin{aligned} d^2(\bar{r}, \bar{k}_0) &= (\bar{r} - (\bar{r}^t \bar{k}_0)\bar{k}_0)^t (\bar{r} - (\bar{r}^t \bar{k}_0)\bar{k}_0) \\ &= \bar{k}^t (I \bar{r}^t \bar{r} - \bar{r}\bar{r}^t) \bar{k}^t \end{aligned}$$

where $\|\bar{k}_0\|^2 = \bar{k}_0^t \bar{k}_0 = 1$ is assumed. In combination with (1)

$$V_f^2 = \bar{k}_0^t \mathbf{J} \bar{k}_0 \tag{3}$$

is obtained with:

$$\mathbf{J} = \begin{pmatrix} J_{11} & -J_{12} & \dots & -J_{1n} \\ -J_{21} & J_{22} & \dots & -J_{2n} \\ \vdots & \vdots & \ddots & \vdots \\ -J_{n1} & -J_{n2} & \dots & J_{nn} \end{pmatrix}$$

where

$$J_{ii} = \int_{E_n} \sum_{j \neq i} x_j^2 |\hat{f}(\bar{r})|^2 dE_n \tag{4}$$

for diagonal elements and

$$J_{ij} = \int_{E_n} x_i x_j |\hat{f}(\bar{r})|^2 dE_n \tag{5}$$

for off-diagonal elements except for a sign change. The minimization problem formulated in (2) is solved by k_0 corresponding to the least eigenvalue of the inertia matrix $\mathbf{J}$ of the Fourier domain, [4]. All eigenvalues are real and the smallest eigenvalue corresponds to this minimum. This matrix contains sufficient information to allow computation of the optimal $\bar{k}_0$ in the sense given by (2)

Lemma 1 *The inertia matrix of the energy of the Fourier domain is possible to compute in the spatial domain by the following relation:*

$$J_{ii} = \frac{1}{4\pi^2} \sum_{j \neq i} \int_{E_n} (\frac{\partial f}{\partial x'_j})^2 dE_n \tag{6}$$

for the diagonal elements and

$$-J_{ij} = -\frac{1}{4\pi^2} \int_{E_n} \frac{\partial f}{\partial x'_i} \frac{\partial f}{\partial x'_j} dE_n \tag{7}$$

for off-diagonal elements. Here x'_j is the spatial domain coordinate corresponding to the Fourier domain coordinate x_j and $dE_n = dx'_1 dx'_2 ... dx'_n$

Proof of the lemma is immediate by applying the Parseval relation and the fact that a differentiation in the spatial domain corresponds to multiplication by the respective coordinate in the Fourier domain, (4) and (5).
Using the previous lemma we have the tools to find an optimal orientation of any image f. The obtained orientation will be unique if all the eigenvalues differ from the least eigenvalue. Moreover the variance given by (1) would be exactly zero if and only if f is a linear symmetric image. When the multiplicity of the least eigenvalue is larger than 1, there is no unique axis $t\bar{k}_0$, by which the image can be described as $g(\bar{k}_0^t \bar{r})$ for some one-dimensional function g. Instead, the energy in the Fourier domain is distributed in such a way that there are plenty of such axes which give the least square error. More exactly these axes are any axes given by a linear combination of the eigenvector space belonging to the least eigenvalue. Here it should be observed that the dimension of this space is equal to the multiplicity of the eigenvalue it corresponds to (the least one). This is due to the fact that **J** is positive semi-definite and symmetric by definition, (1) and (3). In other words, there is no unique and optimal axis passing through the origin but an optimal and unique hyperplane passing through it in the Fourier domain when the multiplicity of the least eigenvalue is greater than one. How shall we interpret the case when the least two eigenvalues of the inertia matrix **J** are equal? If they are equal and vanish?
Since the matrix **J** is symmetric and positive semi-definite, it can be diagonalized by a similarity transformation to $\mathbf{J'}$

$$\mathbf{J'} = \mathbf{P^t J P}$$

This corresponds to a rotation of the coordinate axes (both in the Fourier and the spatial domain). Let the coordinate axes of the spatial domain after rotation be $\hat{u}_1$, $\hat{u}_2 ...$ $\hat{u}_n$. Then by using lemma 1) and $J'_{00} = J'_{11} = \lambda_0$ we obtain

$$\int_{E_n} (\frac{\partial f}{\partial u_0})^2 dE_n = \int_{E_n} (\frac{\partial f}{\partial u_1})^2 dE_n \tag{8}$$

We will call such images perfectly balanced images with respect to $\hat{u}_0$ and $\hat{u}_1$ coordinate axes due to a similar definition in mechanics when $\lambda_0 = \lambda_1$. When $J'_{00} = J'_{11} = 0$ we obtain

through lemma 1)

$$\sum_{i\neq 0}\int_{E_n}(\frac{\partial f}{\partial u_i})^2 dE_n = 0$$

$$\sum_{i\neq 1}\int_{E_n}(\frac{\partial f}{\partial u_i})^2 dE_n = 0$$

Since all elements in the sums above are positive we have

$$\int_{E_n}(\frac{\partial f}{\partial u_i})^2 dE_n = 0$$

for all i, which in turn leads to the fact that

$$\frac{\partial f}{\partial u_i} = 0$$

for all allowed i. But this is the same as saying that f is a constant image. If only one eigenvalue is zero then we have

$$\frac{\partial f}{\partial u_i} = 0$$

for all i except the one corresponding to the zero eigenvalue. That is, it is constant in the directions perpendicular to the axis belonging to the least eigenvalue. Thus when two eigenvalues of the matrix **J** are zero, so are all the others, and by this we have established the following lemma.

Lemma 2 *If one of the eigenvalues of the inertia matrix* **J** *of the Fourier transform of the image f, has value zero then this eigenvalue has multiplicity of either 1 or n. It is equal to 1 if and only if we have a linearly symmetric image, and equal to n if and only if we have a constant image.*

To illustrate the concept of perfectly balanced images we have such a Fourier domain in Figure 1 a). It can, for this image, be shown that any axis through the origin in the Fourier domain will give the same least square error:

$$\sum_{i=1}^{4} m_i d^2(\bar{r}_i, \bar{k}) = 2a^2m^2$$

This is a perfectly balanced image. Thus the 2-D inertia matrix **J** of this case has one eigenvalue $2a^2m^2$ of multiplicity 2. The spatial domain corresponding to this Fourier domain consists of two planar waves (sinusoids) in the directions of the coordinate axes. Interpreting Figure 1 a) in 3 dimensions would give a hyperplane as in Figure 1 b). In the 3–D spatial domain this corresponds to an image as the one in Figure 1 a), in every 2–D plane perpendicular to the axis defined by the vector, $\hat{x}_3$. In Figure 1 a) we obtain both eigenvalues equal, namely $2m^2a^2$, while in the 3-D case, Figure 1 b), we obtain eigenvalues $2m^2a^2$, $2m^2a^2$ and $4m^2a^2$. Thus we can say that the image is perfectly balanced with

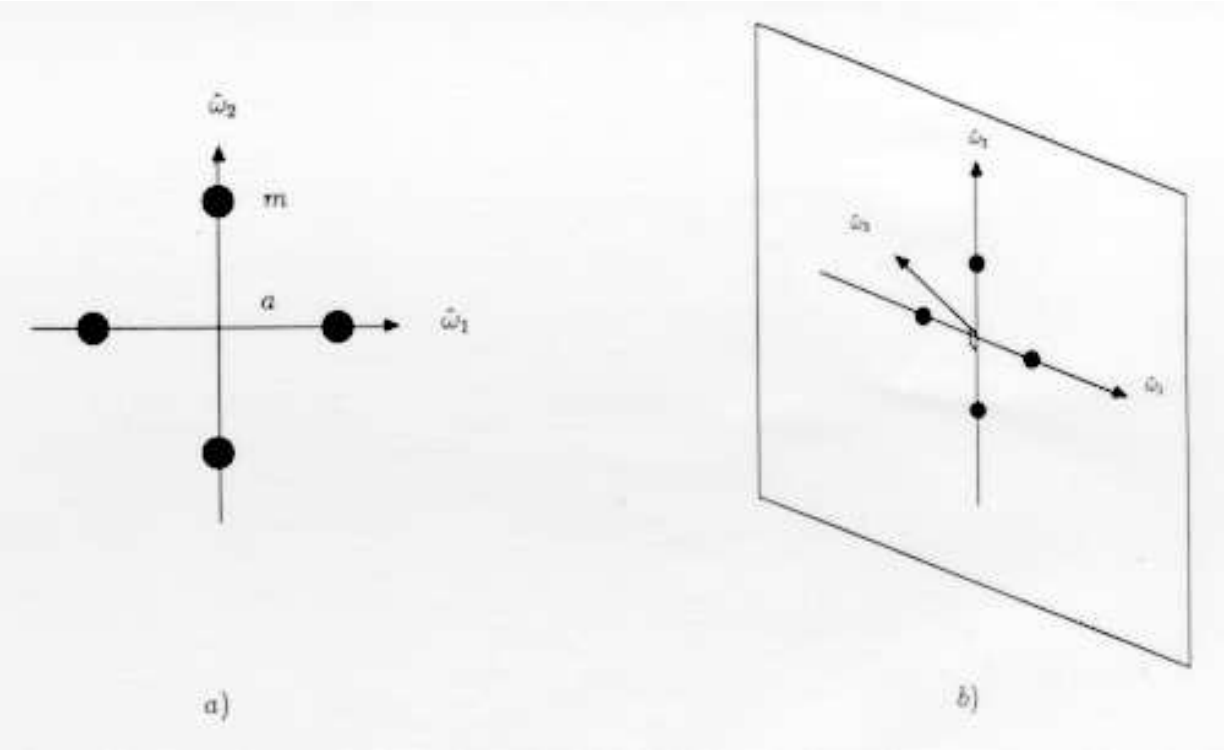

Figure 1: a) and b) illustrate perfectly balanced images in the Fourier domain for 2–D and 3–D respectively. m is energy. A spatial domain image corresponding to both a) and b) is given by: $A\sin(2\pi a u_1) + A\sin(2\pi a u_2)$, where A is a constant and u_1 and u_2 are spatial domain coordinates corresponding to $\hat{x}_1$ and $\hat{x}_2$. It should be observed that the spatial domain image is constant for all u_3.

respect to any axis perpendicular to $\hat{x}_3$. One is tempted to infer that the image should have its iso-gray values as parallel lines, when the least eigenvalue has multiplicity 2 for the 3–D case. However, this is not always true. A counter-example is when we have equal masses (energies) at the Fourier sites: $(\pm 1, \pm 1, 0)$, $(0, 0, \pm\frac{1}{2})$. The eigenvalues are proportional to $\frac{5}{2}$, $\frac{5}{2}$, 4, but this corresponds for instance to three sinusoids in the spatial domain:

$$A\sin(u_1) + A\sin(u_2) + A\sin(\frac{1}{2}u_3)$$

where u_1, u_2, u_3 are coordinates in the three orthogonal spatial domains corresponding to the Fourier coordinates, and A is some constant.

3 2-D implementation of finding the minimum variance axis

To test the theory above we have implemented two algorithms evaluating local orientation of the 2-D images. Both of the algorithms rely on finding the eigenvalues and eigenvectors of the inertia matrix of the Fourier domain. The direction measurements for both of them are the same and based on the eigenvector(s) of the least eigenvalue. They differ on the certainty of the direction estimation. What has been referred to as image in the theory above, becomes a local neighbourhood of the total image in the following discussion. To represent this local image at the point $\bar{r}_j$ we multiply the larger image $f(\bar{r})$, by a window function $w(\bar{r}, \bar{r}_j)$:

$$h_j(\bar{r}) = f(\bar{r})w(\bar{r}, \bar{r}_j). \tag{9}$$

For simplicity we choose w a gaussian:

$$w(\bar{r}, \bar{r}_j) = \exp\,(\,-\frac{4}{d_w^2}\|\bar{r} - \bar{r}_j\|^2) \tag{10}$$

with $\|\cdot\|$ being the Euclidean norm: $\|\bar{r}\|^2 = \bar{r}^t\bar{r}$ and d_ω being a constant controlling the 'diameter' of the local neighbourhood. The algorithm fits a least square error axis in the Fourier domain of the local image h_j corresponding to the least eigenvalues of the inertia matrix of the Fourier domain, $\mathbf{J}$. The computation is pursued in the spatial domain by means of equations (6) and (7). The axis found, $t\bar{k}_0$ is possible to represent by $\bar{k}_0$. Since this is an axis, $-\bar{k}_0$ is an equivalent representation as well. For this reason the orientation of an axis $t\bar{k}_0$ can be defined as $2\phi_0$, if ϕ_0 is the direction angle of $\bar{k}_0 = k_x\hat{x}_1 + k_y\hat{x}_2$:

$$\phi_0 = \tan^{-1}(k_x, k_y) \tag{11}$$

Consequently both $-\bar{k}$ and $\bar{k}$ will be mapped to the same angle, through $2\phi_0$. It can easily be shown that the eigenvalues of $\mathbf{J}$ for the 2–D case, corresponding to h_j are:

$$\lambda_{0,1} = \frac{1}{2}(J_{22} + J_{11} \pm \sqrt{(J_{22} - J_{11})^2 + 4J_{12}^2}) \tag{12}$$

The eigenvector corresponding to the least eigenvalue can be found to be $\bar{k}_0 = k_x\hat{x}_1 + k_y\hat{x}_2$ satisfying:

$$(J_{11} - \lambda_0)k_x - J_{12}k_y = 0 \tag{13}$$

with the Euclidean norm of unity. Thus the orientation becomes:

$$2\phi_0 = 2\tan^{-1}(k_x, k_y) \tag{14}$$

By using[1] (12), (13), and (14)

$$2\phi_0 = \tan^{-1}(J_{22} - J_{11}, 2J_{12})$$

is obtained. Define the complex variable z as:

$$z = J_{22} - J_{11} + \jmath 2J_{12} \tag{15}$$

thus

$$2\phi_0 = \arg z$$

The certainty in this approximation of the local orientation depends on the behaviour of the eigenvalues λ_0 and λ_1, according to the discussion in the previous section. A linear symmetry of the neighbourhood is probable if λ_0 is small relative to λ_1. An 'ideal' linear symmetry occurs when $\lambda_0 = 0$ and $\lambda_1 >> 0$. A certainty measure, C_{f1}, incorporating these properties is

$$C_{f1} = (\frac{\lambda_1 - \lambda_0}{\lambda_1 + \lambda_0})^c = [\frac{\sqrt{(J_{22} - J_{11})^2 + 4J_{12}^2}}{J_{22} + J_{11}}]^c = (\frac{|z|}{J_{22} + J_{11}})^c \tag{16}$$

Here c is a positive constant, the purpose of which is to control the dynamic range of the certainty. C_{f1} is defined to be 0 when $J_{22} + J_{11} = 0$. According to the previous section we then have a constant image and there is not a unique orientation for such images. It attains the maximum value 1 if and only if $\lambda_0 = 0$, because both λ_0 and λ_1 are non–negative. C_{f1} decreases when the difference between the eigenvalues decreases. This property effectively tests whether the multiplicity of λ_0 is 2, in which case there is not a unique orientation minimizing the variance.
An alternative certainty measure is:

$$C_{f2} = \lambda_1 - \lambda_0 = |z| \tag{17}$$

In this measure we do not get a unique certainty value when $\lambda_0 = 0$. Rather the confidence varies due to the largest eigenvalue when this happens. A consequence of this is that when the neighbourhood is linear symmetric with small energy, it is considered as less reliable even though the orientation measurement is correct. This is justified when it is desired that the certainty decreases continuously as the image becomes constant. Both of these certainty measures are considered.

[1] see Appendix B at the end of this chapter

Thus the task is reduced to express either of the certainty parameters C_{f1} or C_{f2} and the orientation estimation $2\phi_0$. The evaluations of these are governed by the equations (17), (16) and (15), which in turn rely on the efficient computation of the elements of the inertia matrix. Computation of these parameters for every neighbourhood in a discrete image is accomplished as follows.
Consider a discrete representation of the 2-D, bandlimited image $f(\bar{r})$. The continuous image can be reconstructed from its discrete samples, f_i by

$$f(\bar{r}) = \sum_i f_i \mu(\bar{r} - \bar{r}_i) \tag{18}$$

where $\mu(\bar{r})$ is an analytic function governing the behaviour of the continuous function between the discrete values. We will call it the interpixel function. μ can be assumed to be known since it is theoretically the inverse Fourier transform of a function which is 1 at the passband of the considered image and 0 at the outside. For its concentration in both Fourier and spatial domains we choose μ as a gaussian as well:

$$\mu(\bar{r}) = \exp\,(\,-\frac{4}{d_p^2}\|\bar{r}\|^2) \tag{19}$$

even though it is not an ideal interpixel function, since it is not strictly bandlimited. Under these conditions an approximation to J_{11} yields:

$$\begin{aligned} J_{11}^j &= \frac{1}{4\pi^2}\int_{E_2}(\frac{\partial h_j}{\partial x_2})^2 dE_2 = \frac{1}{4\pi^2}\sum_i (\frac{\partial f(\bar{r}_i)}{\partial x_2})^2 \times \\ &\int_{E_2} \exp\,(\,-\frac{4}{d_p^2}\|\bar{r} + \bar{r}_j - \bar{r}_i\|^2 - \frac{4}{d_w^2\|\bar{r}\|^2})dE_n \end{aligned} \tag{20}$$

Here $(\frac{\partial f}{\partial x_2})^2$ is reconstructed from its samples

$$(\frac{\partial f(\bar{r})}{\partial x_2})^2 = \sum_i (\frac{\partial f(\bar{r}_i)}{\partial x_2})^2 \mu(\bar{r} - \bar{r}_i) \tag{21}$$

since it is bandlimited as well when f is. This requires that we have a version of $\frac{\partial f}{\partial x_2}$ oversampled by at least a factor 2 in every dimension. This is due to the fact that squaring a bandlimited function doubles its passband in every dimension. This is an effect which can be removed easily by resampling, if necessary. J_{11}^j corresponding to a neighbourhood, characterized by the coordinate vector $\bar{r}_j$ and a window function of "diameter" d_w, is then computed as

$$J_{11}^j = \frac{1}{4\pi^2}\sum_i (\frac{\partial f(\bar{r}_i)}{\partial x_2})^2 m_i^j \tag{22}$$

where m_i^j is given by (20)

$$\begin{aligned} m_i^j &= \int_{E_2} \exp(-\frac{4}{d_p^2}\|\bar{r} + \bar{r}_j - \bar{r}_i\|^2 - \frac{4}{d_w^2}\|\bar{r}\|^2)dE_2 \\ &= \frac{\pi}{4}\frac{d_p^2 d_w^2}{d_p^2 + d_w^2}\exp\,(\,-\frac{4}{d_p^2 + d_w^2}\|\bar{r}_j - \bar{r}_i\|^2) \end{aligned} \tag{23}$$

(22) is nothing but a convolution of the discrete version of the $(\frac{\partial f}{\partial x_2})^2$ by a gaussian. Since the gaussian decreases rapidly outside of a circle with the radius $\sqrt{d_p^2 + d_w^2}$, we can truncate it when it is sufficiently small. In our experiments this is done when it has decreased to about 1% of its maximum. Similarly J_{11}^j, J_{22}^j and J_{12}^j can be approximated by averaging the discrete images:

$$\begin{aligned} J_{22}^j &= \frac{1}{4\pi^2} \sum_i (\frac{\partial f(\bar{r}_i)}{\partial x_1})^2 m_i^j \\ J_{12}^j &= \frac{1}{4\pi^2} \sum_i \frac{\partial f(\bar{r}_i)}{\partial x_1} \frac{\partial f(\bar{r}_i)}{\partial x_2} m_i^j \end{aligned} \tag{24}$$

Thus z for the point $\bar{r}_j$ becomes:

$$\begin{aligned} z^j &= \frac{1}{4\pi^2} \sum_i [(\frac{\partial f(\bar{r}_i)}{\partial x_1})^2 - (\frac{\partial f(\bar{r}_i)}{\partial x_2})^2 + 2\jmath \frac{\partial f(\bar{r}_i)}{\partial x_1} \frac{\partial f(\bar{r}_i)}{\partial x_2}] m_i^j \\ &= \frac{1}{4\pi^2} \sum_i (\frac{\partial f(\bar{r}_i)}{\partial x_1} + \jmath \frac{\partial f(\bar{r}_i)}{\partial x_2})^2 m_i^j = \frac{1}{4\pi^2} \sum_i u_i m_i^j \end{aligned} \tag{25}$$

where u_i is the complex valued image obtained by taking the square of the gradient of the image, interpreted as a complex number instead of a real vector:

$$u_i = (\frac{\partial f(\bar{r}_i)}{\partial x_1} + \jmath \frac{\partial f(\bar{r}_i)}{\partial x_2})^2. \tag{26}$$

Similarly

$$J_{11}^j + J_{22}^j = \frac{1}{4\pi^2} \sum_i |u_i| m_i^j \tag{27}$$

is obtained. Thus calling the discrete image defined by (26) as u and the filter defined by (23) as m we have:

$$\begin{aligned} 2\phi_0 &= \arg(u * m) \\ C_{f1} &= \frac{|u * m|^c}{(|u| * m)^c} \\ C_{f2} &= \frac{1}{4\pi^2} |u * m| \end{aligned} \tag{28}$$

where the symbol $*$ represents the usual convolution operation. Here $\arg(\cdot)$, $|\cdot|$ and $(\cdot)^c$ operations are assumed to be applied pointwise to their arguments and thus $2\phi_0$, C_{f1} and C_{f2} become images representing local orientation and certainties. The first algorithm is to evaluate $2\phi_0$ and C_{f1} and the second algorithm to evaluate $2\phi_0$ and C_{f2}.
The discrete partial derivatives necessary for the evaluation of u can be produced by convolution with various filters. For the sake of completeness we just mention the technique

used before: Expansion of the image in its interpixel functions and application of the derivative operation.

$$(\frac{\partial f(\bar{r}_j)}{\partial x_1}) = \sum_i f_i \frac{\partial}{\partial x_i} \mu(\bar{r}_j - \bar{r}_i) \tag{29}$$

As before this gives us a filter which decreases rapidly outside of a small region close to the examined point $\bar{r}_j$. The evaluation of (29) and (28) is easily computed on hardware with support for convolution. In the experiments below a GOP–300 computer has been used.

4 Experimental results

In the experiments, the implementation proposed in the previous section has been tested for detection of the linear symmetric neighbourhoods. This is carried out in two steps:
1) Evaluate a partial derivative picture. In reality the complex variable u_j of the neighbourhood at the point $\bar{r}_j$,

$$\frac{\partial f(\bar{r}_j)}{\partial x_1} + \jmath \frac{\partial f(\bar{r}_j)}{\partial x_2}$$

is computed by using (29) and then this complex number is squared.
2) Estimate local orientation, $2\phi_0$, and the certainty of this estimation, either of C_{f1} or C_{f2} according to (28) based on the image obtained in step 1).
Figure 2 shows an image containing all possible directions for sine waves with exponentially increasing frequency in the radial direction of the circles. Gaussian uncorrelated white noise is added to the right half of the image with the proportion 1:3 that is $0.25 f_i + 0.75 Y_i$ where f_i is the image intensity and Y_i is the stochastic variable with the distribution of N(0,32). In the experiments this proportion is varied and the local orientation is examined for different sizes of filters in the two steps mentioned before. In general it could be observed that the filter size of the first step affects the accuracy of the orientation detection more than the size of the neighbourhood given by the gaussian, (23), in the second step. This is not surprising, because the probability that the energy at a high frequency is erroneous is higher than the same probability for a low frequency. The reason is that most of the natural errors are composed of high frequencies like aliasing error, discretization error, measurement error, etc. A squaring of the gradient image causes these errors to propagate to lower parts of the local frequency spectrum.This makes it difficult to remove the noise by increasing the filter size, i.e. low pass filtering. Figure 3 shows the orientation estimation of the profile of the test image cut along the line passing through the origin of the circles shown in Figure 2. The profiles at the left part of the test circles demonstrate these phenomena. Both profiles should have constant levels, since the orientation of the profile is constant. The shown two profiles are due to two different filter configurations of two estimations. Profile 1 is due to a 9×9 filter in the first and a 15×15 gaussian averaging filter in the second step. The second profile shows the result of a 5×5 gaussian derivative filter at the first step and 21×21 at the second step. It can be observed that in the latter filter configuration the effect of the noise is removed at low and medium frequencies while at high frequencies the orientation estimate is not as good as at the lower frequencies.

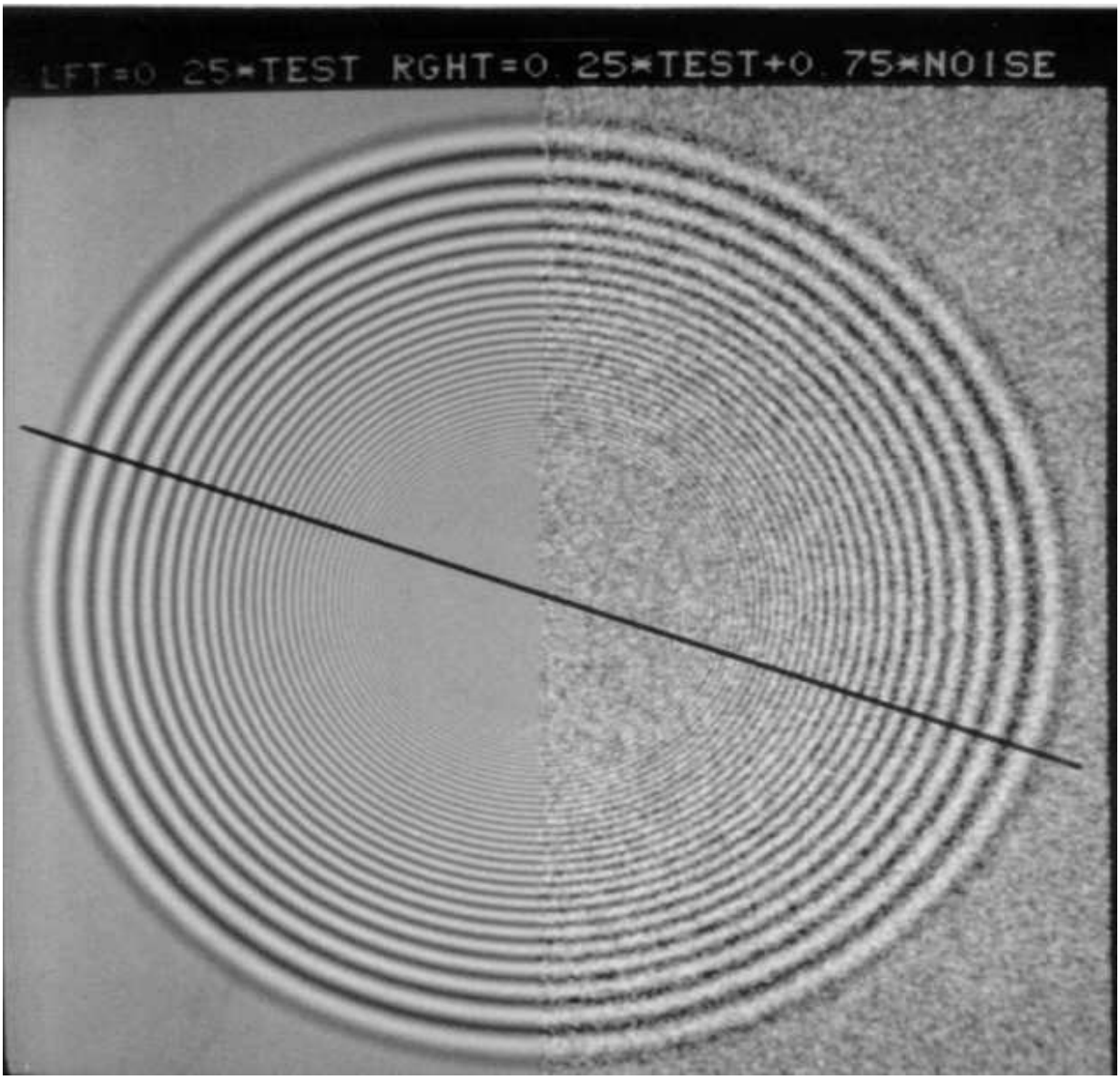

Figure 2: The test image used in the experiments. The straight line is the line along which the profiles of results are presented at the proceeding figures.

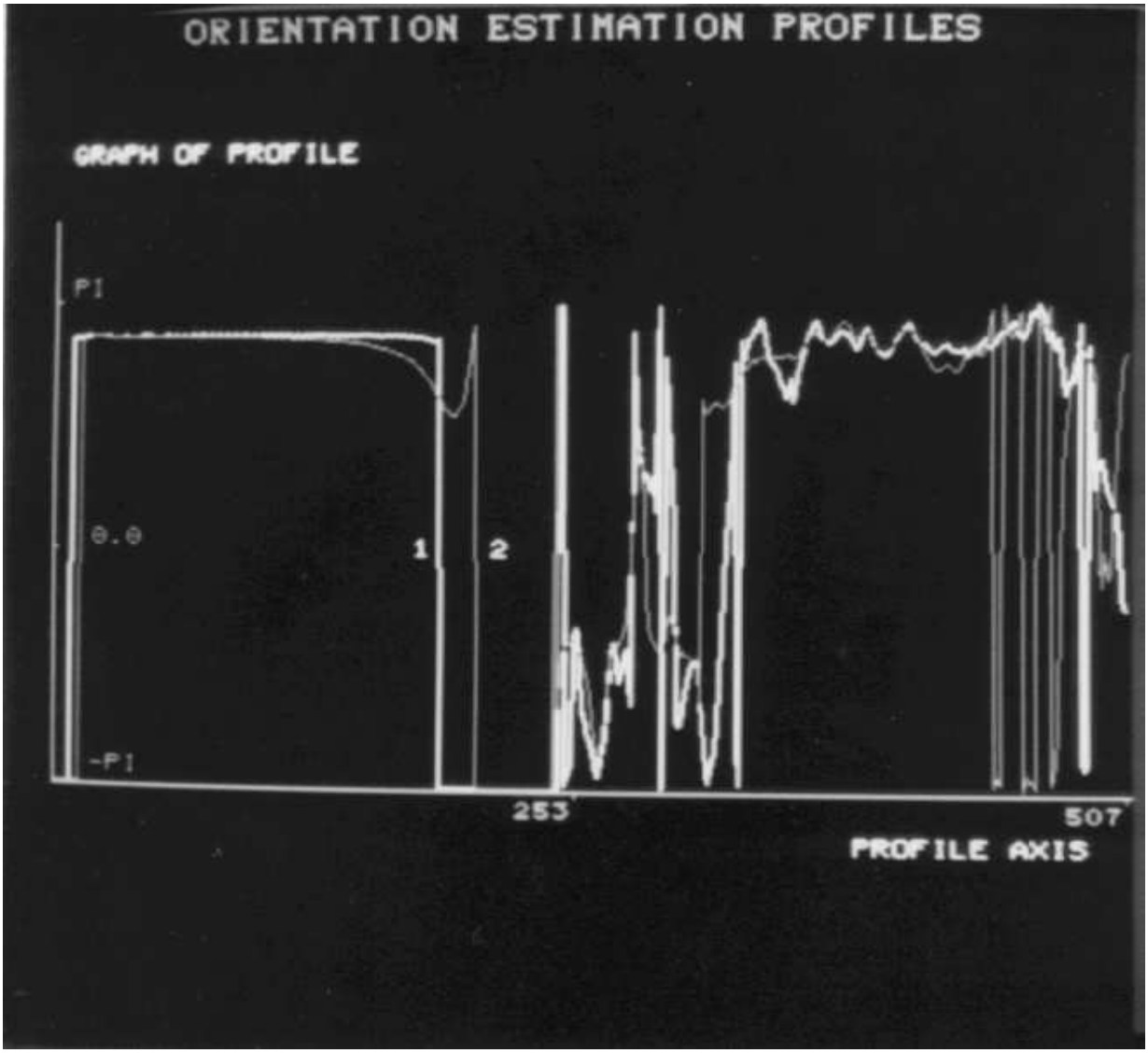

Figure 3: Orientation estimation with two different filter configurations. Graph 1 illustrates 9×9 and 15×15 configuration at the two steps of the algorithm, while 2 is due to 5×5 and 21×21 configuration.

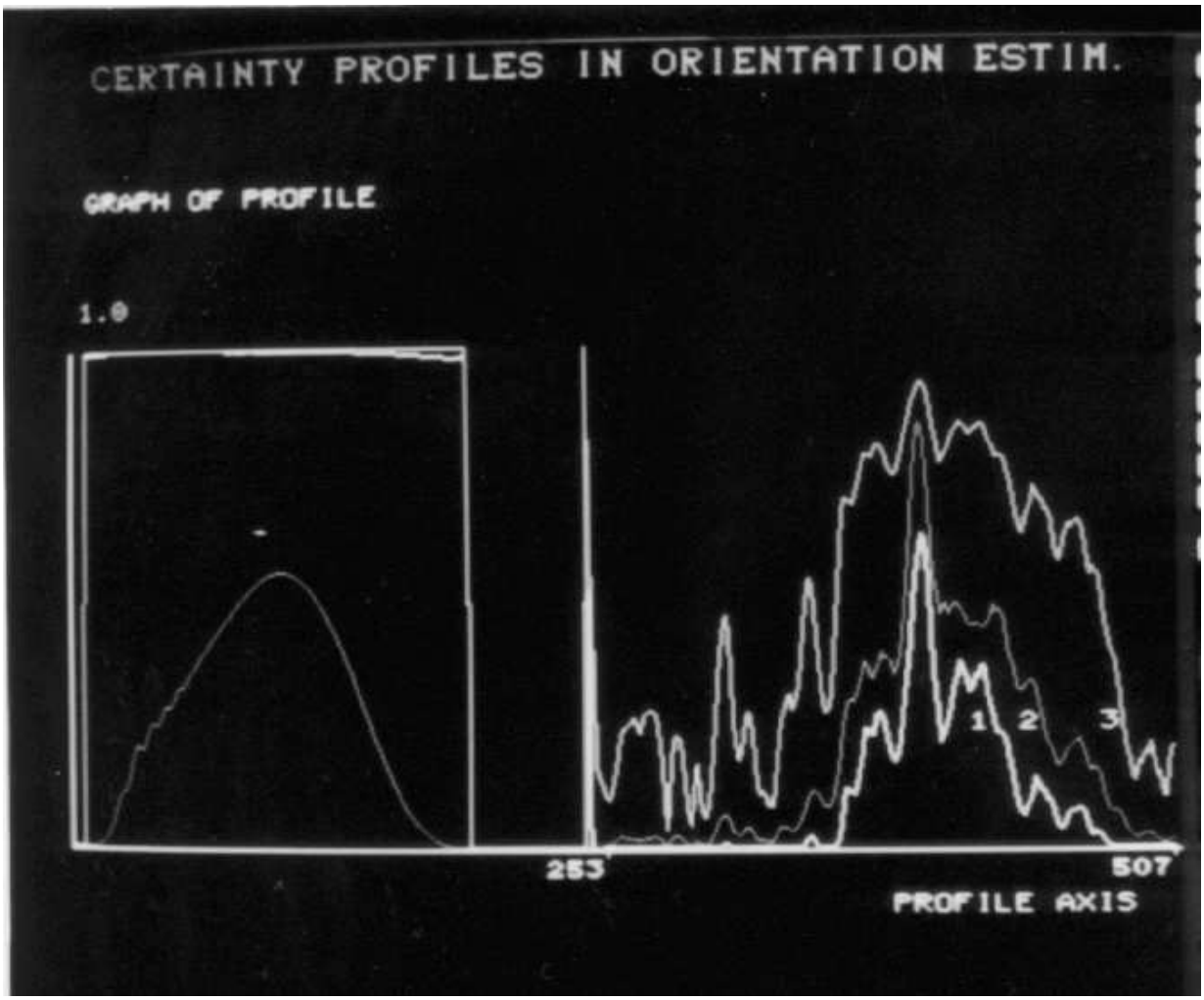

Figure 4: Certainty measures for the profile 1 in Figure 3 Graphs 1 and 3 are due to C_{f1} with $c = 6$ and $c = 1$ respectively, while 2 corresponds to C_{f2}.

Control of the certainty in the presence of noise without disturbing the certainty in the less noisy parts is a desirable feature for many applications. Profiles in Figure 4 show the certainty measures C_{f1} and C_{f2} of the estimation given by profile 1 in Figure 3. Profiles 1 and 3 correspond to C_{f1} with c=6 and c=1 respectively. C_{f2} is given by profile 1. Since this measure is not a relative measure like C_{f1}, it has a high degree of frequency dependence. It is considerably more 'suspect' outside of the pass band, compared to the one given by profiles 1 and 3. A natural consequence of this is that the fluctuations in the noisy part of the image are small with a low level certainty. The frequency sensitivity band of the certainty parameter C_{f2} is due to the derivation in the first step, and averaging in the second step. In the Fourier domain this corresponds to a multiplication of an increasing and a decreasing function at low frequencies. The center frequency can thus be varied by varying the scale of the filters at the two steps, Figure 5. This certainty measure can be

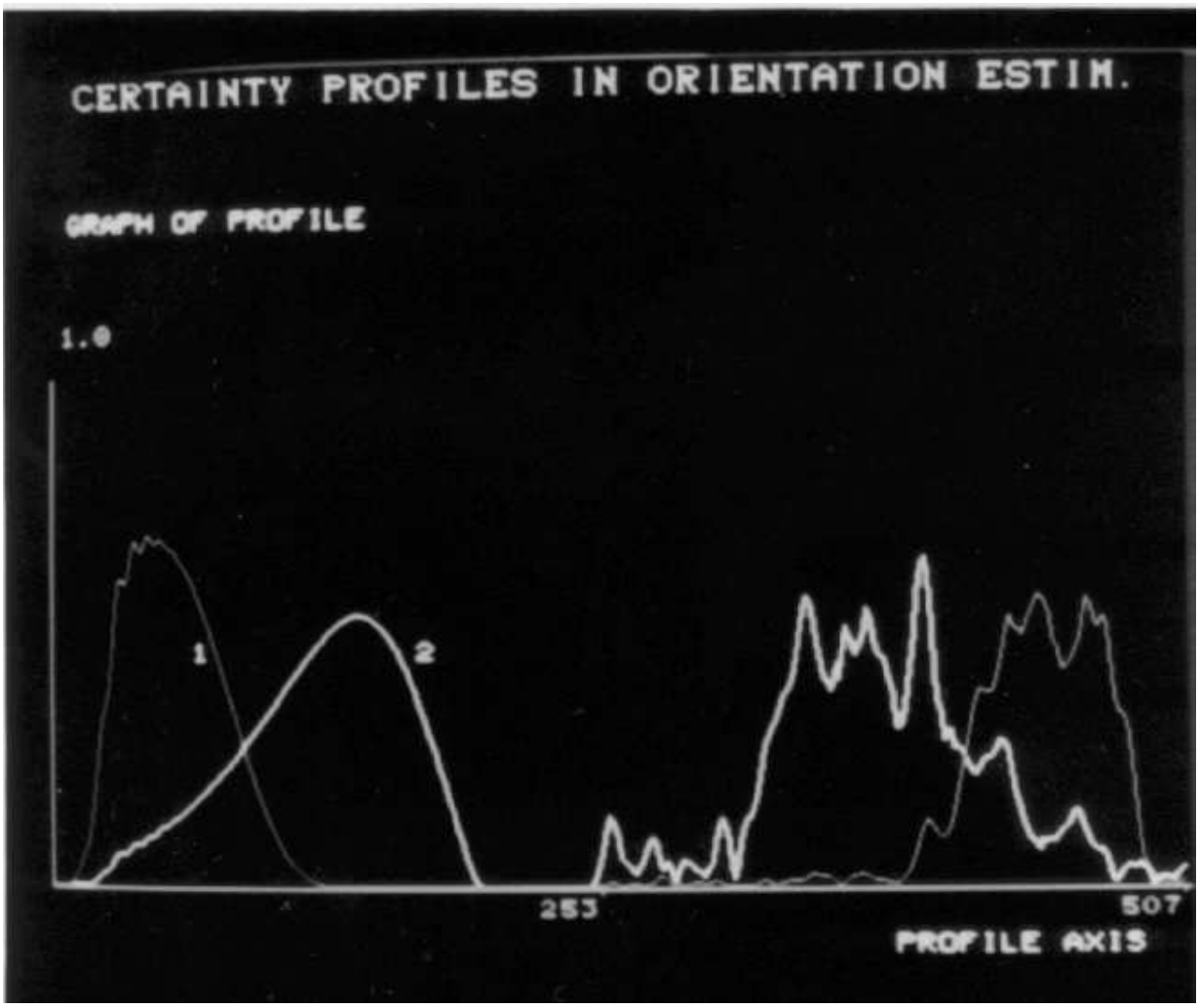

Figure 5: Frequency dependence of C_{f2}. Graph 1 corresponds to 15×15 and 21×21 configuration at the two steps of the algorithm. 2 corresponds to 5×5 and 19×19 configuration.

used when it is desirable to control the orientation measurements for the neighbourhoods with a priori known frequencies.

5 Conclusion

It is experimentally verified that the problem of orientation detection within a local neighbourhood is possible to solve in the Fourier domain for the 2–D case. The problem for the 3–D case is possible to solve in a similar way. The first section is sufficiently general to handle the 3–D problem, while Section 2 uses some fundamental properties of the 2–D case and its relation to the complex z–plane to accomplish the representation of orientation and the certainty of the estimation. The proposed certainties C_{f1} and C_{f2} and the orientation $2\phi_0$ are shown to be computable by averaging the complex valued image u which is the square of the gradient represented in the complex form. For the first algorithm producing C_{f1} and $2\phi_0$, 5 real convolutions are required, while in the second algorithm producing C_{f2} and $2\phi_0$ 4 real convolutions are required. In both cases the algorithms can, under the condition that f is bandlimited, be summarized in the compact forms: $\frac{m*(\nabla*f)^2}{m*|\nabla*f|^2}$ and $m*(\nabla*f)^2$ with ∇ being the complex gradient filter given by $D_{x_1}+\jmath D_{x_2}$, and m the averaging filter. The resulting complex image can be seen and interpreted directly on a colour TV monitor, if the magnitude of the image corresponding to the certainty controls the intensity, and the argument corresponding to the orientation controls the colour [7].
One of the reasons for first evaluating a 2–D implementation, apart from it having less data compared to 3–D, is the difficulty of displaying the orientation of 3-D images together with the certainties of the given orientation estimation. The experimental work indicates clearly that, for higher dimensions, it is possible to evaluate the local orientation accurately together with its certainty with controllable behaviour when noise is present. The first section shows that even though there is no obvious linear symmetry in the neighbourhood considered, the estimation found is optimal in the least squares sense.

Acknowledgements

The authors would like to express their gratitude to the other members of the Computer Vision Laboratory group for valuable discussions and to the STU for the financial support.

References

[**1**] H. Knutsson: "Filtering and reconstruction in image processing." Dissertation No. 88, 1982, Linköpings Studies in Science and Technology, Linköping University, Sweden.

[**2**] R. Lenz: "Optimal filtering." Linköping university, Internal Report of the Department of Electrical Engineering, 1985.

[**3**] Robert A. Hummel: "Feature Detection Using Basis Functions." Computer Graphics and Image Processing 9, 1979.

[**4**] A. Wouk: "A course of applied functional analysis." Wiley, New York, 1979.

[**5**] J. Bigün, G.H. Granlund: "Central symmetry modelling" proc. EUSIPCO–86 part 2 pp 883–886

[**6**] J. Bigün: "Circular symmetry models in image processing" Licentiate report no: 85 1986 Linköping studies in science and technology

[**7**] G.H. Granlund: "In Search of a General Picture Processing Operator." Computer Graphics and Image Processing 8, 155–173 (1978).

[**8**] G.H. Granlund: "Hierarchical Image Processing." Proceedings of SPIE Technical conference, Geneva, April 18–27, 1983.

[**9**] P.E. Danielsson: "Rotation invariant linear operators with directional response." Proceedings of 5'th international conference on pattern recognition, December 1980.

[**10**] I.L. Meriam: "Statics." John Wiley & Sons, New York, 1980.